Comparison of Different Classification Approaches for Land Cover Classification using Multispectral and Fusion Satellite Data: A Case Study in Ören Forest Planning Unit

Alkan GÜNLÜ[1*]

[1] Çankırı Karatekin University, Faculty of Forestry, Department of Forestry Engineering, 18200, Çankırı

Abstract

In this study, the success of different satellite images and classification approaches in land cover (LC) classification were compared. A total of six satellite images, including two passive (Landsat 8 OLI (L8) and Sentinel-2 (S2)) satellite images and four fused satellite images from active (Sentinel-1(S1)-VH and VV polarization) and passive satellite images (L8-S1-VH, L8-S1-VV, S2-S1-VH and S2-S1-VV) were used in the classification in the study. For this purpose, L8, S2, L8-S1-VH, L8-S1-VV, S2-S1-VH and S2-S1-VV satellite images were classified according to three ((Maximum Likelihood Classification (MLC), Support Vector Machine (SVM) and Artificial Neural Networks (ANN)) different image classification approaches using the forest cover types map as gorund data. The results obtained from classification methods were evaluated based on overall accuracies (OA) and kappa coefficients (KC). When the classification successes obtained from the three classification methods are evaluated, it was observed that the KC ranged from 0.66 to 0.95 and the OA ranged from 76.82% to 96.67. The results indicated that the highest OA was displayed by MLC (ranged 85.33% to 96.67%), closely followed by SVM (ranged 80.11% to 91.93%), and finally ANN (ranged 76.82% to 89.92%). In addition, a comparison of classification performance using three utilized classification algorithms was performed. The S1-VH; S1-VV and, S2 and L8 fused images classified with an MLC algorithm produce the most accurate LC map, indicating an OA of 92.00%, 94.00%, 96.67%, 93.33% and a KC of 0.90, 0.93, 0.95, 0.92 for S2 and L8, respectively. Thus, it can be concluded that fused of satellite images improve the accuracies of LC classification.

Keywords: Land cover classes, maximum likelihood classification, support vector machine, artificial neural networks, remote sensing data.

Multispektral ve Birleştirilmiş Uydu Görüntüleri Kullanılarak Arazi Örtüsü Sınıflandırılmasında Farklı Sınıflandırma Yaklaşımlarının Karşılaştırılması: Ören Orman İşletme Şefliği Örneği

Öz

Bu çalışmada, arazi örtüsünün sınıflandırılmasında farklı uydu görüntüleri ve sınıflandırma yaklaşımlarının başarıları karşılaştırılmıştır. Çalışmada iki pasif (Landsat 8 OLI (L8) ve Sentinel-2 (S2)) uydu görüntüsü ile birlikte aktif (Sentinel-1 (S1)-VH ve VV polarizasyonlu) ve pasif uydu görüntülerinin birleştirilmesiyle elde edilmiş (L8-S1-VH, L8-S1-VV, S2-S1-VH ve S2-S1-VV) dört uydu görüntüsü olmak üzere toplam altı uydu görüntüsü sınıflandırmada kullanılmıştır. Bu amaçla, L8, S2, L8-S1-VH, L8-S1-VV, S2-S1-VH ve S2-S1-VV uydu görüntüleri yersel veri olarak meşcere tipleri haritası kullanılarak üç farklı görüntü sınıflandırma ((maksimum olasılık sınıflandırması (MOS), Destek Vektör Makineleri (DVM) ve Yapay Sinir Ağları (YSA)) yaklaşımına göre sınıflandırılmıştır.Üç sınıflandırma metodundan elde edilen sınıflandırma başarıları değerlendirildiğinde, Kappa Katsayı (KK)'nın 0,66 ile 0,95, Genel Doğruluğun (GD) ise %76,82 ile 96,67 arasında değiştiği görülmüştür. En yüksek GD'nin MOS ile (%85,33 ile %96,67 arasında), sonra DVM (%80,11 ile %91,93 arasında) ve son olarak YSA (%76,82 ile %89,92 arasında) olduğunu görülmüştür. Bununla birlikte, kullanılan üç sınıflandırma yaklaşımının başarıları karşılaştırılmıştır. Birleştirilmiş S2-S1-VH, S2-S1-VV, L8-S1-VH ve L8-S1-VV uydu görüntüleri ile MOS sınıflandırma yaklaşımında sırasıyla en iyi GD (92.00%, 94.00%, 96.67%, 93.33) ve KK (0.90, 0.93, 0.95, 0.92) değerleri sırasıyla elde edilmiştir. Elde edilen sonuçlar değerlendirildiğinde, birleştirilmiş uydu görüntülerinin kullanılması arazi örtüsü sınıflandırmasının başarısını artırdığı görülmüştür.

Anahtar Kelimeler: Arazi örtüsü sınıfları, maksimum olasılık sınıflandırması, destek vektör makinesi, yapay sinir ağları, uzaktan algılama verisi.

*Corresponding Author (Sorumlu Yazar):

Alkan GÜNLÜ (Doç. Dr.); Çankırı Karatekin University, Faculty of Forestry, Department of Forestry Engineering, 18200, Çankırı-Türkiye. Tel: +90 (376) 212 2757, Fax: +90 (376) 213 6983, E-mail: alkangunlu@karatekin.edu.tr
ORCID: 0000-0003-4759-3125

1. Introduction

Land Cover (LC) studies are a substantial factor for many types of research including the earth's surface (Ban et al. 2015). The LC mapping, which provides important information on various topics such as assessment of land-use dynamics, ecosystem services, global climate change, development of land use policy, is an important data source for forest ecosystem planners (Fry et al., 2012; Burkhard et al., 2012; Gebhardt et al., 2014; Guidici and Clark, 2017; Noi and Kappas 2018; Hussain et al., 2019). Remote sensing data are the basic tools utilized to provide information from the ground surface to determine LC classification. It offers the benefit of fast data obtain of LC information at a lower charge and time-comsuming than ground measurements (Pal and Mather 2004; Szuster et al. 2011; Kuemmerle et al., 2013).

Generally, the LC maps are produced depend on satellite image classification techniques (Topaloğlu et al., 2016; Khatami et al., 2016). Therefore, the LC mapping broadly used optical (e.g., Szuster et al., 2011; Srivastava et al., 2012; Büyüksalih, 2016; Mohajane et al., 2018; Juliev et al., 2019), radar (Miettinen and Liew, 2011; Hütt et al., 2016; Wei et al., 2016; Camargo et al., 2019) and the integration of optical and radar satellite image (Soria-Ruiz et al., 2010; Lu et al., 2012; Fonteh et., 2016; Sirro et al., 2018) satellite images for LC classification and mapping.

There are many parametric ((e.g., Maximum Likelihood Classification (MLC)) and nonparametric ((e.g., Support Vector Machine (SVM) and artificial neural networks (ANN)) classification techniques used to classify LC classes using remote sensing data (Bulut and Günlü, 2016; Shivakumar and Rajashekararadhya, 2018; Abdikan, 2018; Xie et al., 2019). The most broadly performed parametric classification technique is MLC (Srivastava et al., 2012). It depends on the hypothesis that the distribution training data are normally distributed in a special feature area (Lillesand et al., 2004). The Support Vector Machine (SVM) is a broadly utilized machine learning algorithm in satellite images by maintaining high accuracy as using minor ground data sets (Mountrakis et al., 2011). In contrast to MLC, the ANN does not base on the normal distributed data assumption (Dixon and Candade, 2008; Szuster et al., 2011). The ANN approach, which have been performed on satellite images in recent years, generally for LC classification (Yuan et al., 2009; Pradhan et al., 2010; Ridwan et al., 2017; Şerifoğlu Yılmaz et al., 2018; Ullah et al., 2019).

When the literature studies on the subject are examined, there are many studies carried out for determining LC classes by using different classification techniques with different satellite images. Günlü et al. (2008) mapped LC classes in the Ormanustu forest planning unit using of MLC classifier using Landsat 7 ETM+ satellite image and obtained an overall accuracy (OA) of 89.0%, and a kappa coefficient (KC) of 0.86. Li et al., (2011) used a Landsat TM satellite image to classify LC in Brazil by using the MLC approach with a KC of 0.74 and an OA of 77.2%. Shivakumar and Rajashekararadhya (2018) has applied the MLC approach for the LC classification in India using L8 satellite data, indicating a KC of 0.74 and an OA of 88.75%. Yousefi et al., (2015) applied Landsat ETM satellite images in three field areas (Shahreza, Taft and Zarand) in Iran and obtained an OA of 92.8%, 99.96%, 97.1% and a KC of 0.85, 0.99, 0.94, respectively. Ridwan et al., (2017) utilized the SVM approach depend on L8 satellite image to classify LC in the catchment area of Mangkauk and found that the value of OA was 97.22% with KC 0.96. Şerifoğlu Yılmaz et al., (2018) compared to a classification approach to classify LC using a WorldView-2 Multispectral satellite image in Turkey and found that the SVM (OA of 72.38% and KC of 65.31) better results than the ANN (OA of 70.25% and KC of 62.99) approach. Morgan et al. (2015) applied MLC, SVM, and ANN approach to classify LC classes from Landsat 7 ETM satellite image in the northern part of the Nile Delta. They found that the OA of 80.28 %, 80.64%, respectively. In addition, a satisfactory classification success was not achieved with the ANN method in this study. The Sentinel-1 imagery was used by Rao and Kumar (2017) to compared different classification approaches (Isodata, MLC, SVM, ANN, minimum distance, parallelepiped and K-means) for LC classification and stated that the SVM better performance for Sentinel-1 satellite imagery. Many previous studies showed that combinations of spectral and spatial properties increase classification accuracy (Han et al. 2012; Lu et al. 2014). Mushore et al., (2017) applied the SVM approach to improve the LC classification using vegetation indices and bands obtained from L8 in Harere region. As a result of the study, the classification obtained by evaluating the bands and indices together gave higher accuracy classification results than the results obtained by using the individual the bands. In addition to, it has been observed that the images obtained by integrating the active and passive satellite images increase the classification success in determining LC classes (Bagan et al., 2012; Hong et al., 2014; Clerici et al., 2017). Erasmi and Twele (2009) applied Envisat and Landsat ETM+ satellite image for LC classification in Indonesia. They found that texture properties obtained from Envisat SAR image combined with visible and near infrared bands generated from Landsat ETM+ satellite image increased the classification success. The Landsat TM and ALOS PALSAR satellite image were used by Sirro et al., (2018) to classify LC classes in Southern Mexico using the SVM approach. The classification success obtained in the study was

found to increase by one percent. The fused satellite image achieved a one percent advancement in the OA. Tavares et al., (2019) applied a random forest approach for LC classification in the integration of S1 and S2. Their results demonstrated that the best overall accuracy was found for the combining of S1 and S2 (91.07%). However, in a study by Fonteh et al., (2016) used the Sentinel-1 and L8 satellite image to extract LC classes in Cameroon. The fused satellite data indicated no important differences in OA (88.71% and 88.59%, respectively). However, more studies are still required to achieve better classification success using different satellite data and classification approaches. Furthermore, there are not investigated studies that fused the L8; S2 and, S1-VH; S1-VV satellite data with different classification approaches for LC classification in forestry applications in Turkey.

We evaluated the contribution of S1-VH; S1-VV and, L8 and S2 MS satellite image LC classification in the Ören forest planning unit, Turkey. Our main aims are: (i) to determine the OA and KC of the LC classes of the MLC, SVM and ANN approaches by using Multispectral (MS) satellite images (ii) to identify the OA and KC of LC classes of the MLC, SVM and ANN approaches by using fused satellite images (iii) to compare the classification achievements of LC classification of the MLC, SVM and ANN approaches by using both MS and fused satellite images.

2. Material and Methods

2.1. Study area

Ören planning unit is located within the boundary of the Ankara Regional Directorate of Forestry of Turkey (453830–467247 E. 4533948–4544443 N. WGS 84 datum zone 36 N, Figure 1). The elevation ranges from 650 to 1770 m above sea level and the mean elevation is 1300 m. The mean annual temperature and precipitation of the case study area are 11.1 °C and 468.7 mm, respectively. The study area is 7143.6 ha. 5937.8 ha (83.1%) of this area is a forested area, 14.5 ha (0.3%) of this area is treeless forest area and the remaining area 1191.3 ha (16.6%) is non-forested areas (agriculture and settlement). The study area selected is a complicated mixed stand. The main tree species in the case study area are *Pinus brutia, Pinus nigra, Pinus silvestris, Abies bormülleriana, Fagus orientalis, Carpinus orientalis, Quercus pubences* and *Juniperus sp.* (Anonymous 2018).
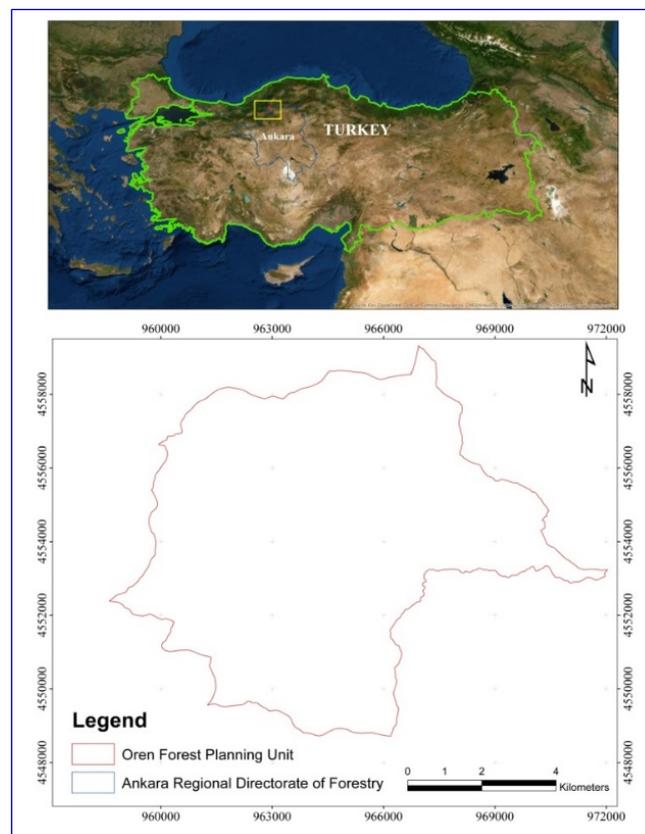

Figure 1. Study area.

2.2. Satellite data and pre-processing

We used S1 SAR dual-polarization (VH-VV) and, the S2 and L8 MS satellite images for LC classes in this study. The S1 and S2 (with cloud-free as Level 1C) were downloaded for free from https://search.asf.alaska.edu/#/ and www.usgs.gov. on 15-August-2018, respectively. The L8 (Level 1T) satellite image with cloud free over the study area (Path 177, Row 32) acquired for free from www.usgs.gov. on 29-August-2018. The satellite images were pre-processed before classification.

2.3. Sentinel-1 and Sentinel-2 image processing

The radiometric and terrain calibration, and speckle reduction were applied to the S1 (VH and VV polarization) image. It was filtered with Lee Sigma (5 x 5 window size). A range of doppler terrain correction together a digital elevation model (30 m) to the terrain correction has been applied. The values (digital number) were transformed to backscattering values (dB). All preprocessing in S1 image has been conducted in the SNAP software. The images (VH and VV) were cut according to the border of the study area and made ready for analysis. Four spectral bands (blue, green, red, and NIR) from S2 satellite images were used for the classification steps in this study. The bands were integrated with the ENVI software using the layer stacking module. The satellite image was downloaded as Level-1C, which involves geometric and radiometric correction on a Universal Transverse Mercator (UTM, Zone 36 N, WGS84) projection. Also, the S2 Level-1C ensures the top of the atmosphere reflectance. The image was cut according to the border of the study area and made ready for analysis.

2.4. Landsat 8 OLI image processing

Six spectral bands (red, green, blue, NIR, SWIR1 and SWIR2) from L8 satellite image were used for the classification stage in this study. It were combined in the ENVI software using the layer stacking module. Due to the satellite image used in the study was obtained from Level 1T, there is no need for any geometrical and atmospheric corrections. Also, atmospheric correction is not required such as image classification for the single satellite image (Srivastava et al. 2012). In addition, the satellite image was imported by using ENVI software and the image geo-referencing accuracy was checked with a topographic map at 1/25.000 scale of the study area. The raw digital number was converted to the radiance values for L8 satellite image. The image was cut according to the border of the study area and made ready for analysis.

2.5. Integration of Sentinel 1A and, Sentinel-2A and Landsat 8 OLI satellite Images

The S1-VH; S1-VV, S2 and L8 satellite images were rectified to the same UTM (Zone 36 N, WGS84) projection. Image fusion is always utilized in the combination of a multi-resolution image to improve visual explication and to increase classification performance (Lu and Weng 2007; Lu et al. 2012). There are a lot of data fusion techniques (such as wavelet-merging technique and principal component analysis) used to improve spatial and spectral information in satellite images (Lu et al. 2012). The wavelet-merging technique is commonly applied in developing LC classification (Lu et al. 2007). Therefore, the technique was applied in this study. In the image fusion process of S1 data and L8; S2, both VH and VV polarization data were applied separately. Furthermore, to merge the L8 bands and S1-VH and S1-VV images into two new satellite image with a spatial resolution of 10 m. Then, two satellite images were obtained by combining the S1-VH and S1-VV images with the bands of the S2 satellite image. In this way, the four different satellite images were obtained.

2.6. Determination of land cover classes

Forest management plans in Turkey are prepared for 10 or 20 year period. In this context, the forest management plan of the study area was renewed in 2018. In this study, LC classes were produced from Forest Cover Type Map (FCTM) with Geographic Information Systems (GIS). LC in the case study area was classified into five types: Conifer Forest (CF), Broadleaf Forest (BF), Mixed Forest (MF), Degraded Forest (DF) and Other (Agriculture and Settlement) areas depend on FCTM. LC classes and information about these classes are given in Table 1. Also, the map produced for LC classes using GIS is shown in Figure 2.

Table 1. Description of land cover classes used in this study.

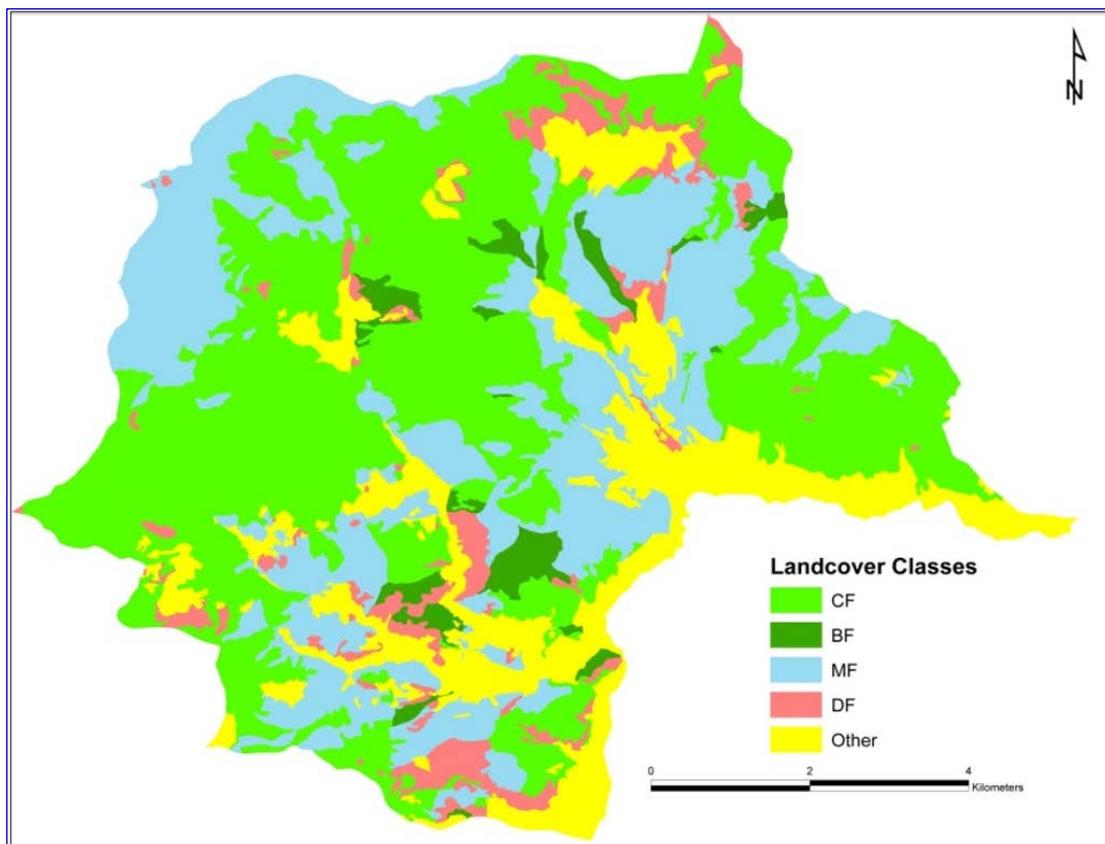| LC	Class Definition	Area (ha)	%
CF	Forest area is consist of pure conifer trees	3341.8	46.8
BF	Forest area is consist of pure broadleaf trees	218.3	3.0
MF	Mixed (CF-BF, BF-CF) forest areas	1961.2	27.4
DF	Degraded forest areas with predicted < 10% tree crown cover	408.9	5.7
Other	Agriculture and settlement areas	1213.4	17.1
	Total	7143.6	100

Figure 2. The map of land cover classes.

3. Classification approaches

The LC class map was used as ground reference data (FCTM) in the classification process. Sample signatures were selected from each LC class by overlapping the LC classes map and satellite images and ten sample signatures were selected for each class depending on the homogeneity of the LC class. Three different classification algorithms were applied in this study. Detailed information on the approaches to this classification are given below.

3.1. Maximum likelihood classification

The MLC method, satellite common in the classification of images a supervised classification that is in use technique (Jia et al. 2011). This method is a statistical-based classification algorithm, average with values,

variance, and covariance that takes into account their values. This class control during the evaluation phase with normal data sets assumed to have distribution. Probability density functions at the classification stage are calculated and the pixels to be classified are assigned to higher classes.

3.2. Support vector machine

The SVM is based on the structural risk minimization principle and statistical learning theory. It initially has two classes for the classification of linear data is designed. Then, it was developed to solve the linear classification problem of non-multi-class series. Purpose in SVM, the most suitable hyper level that can separate the two classes is to obtain. With the hyper level obtained distance between support vectors is maximized and the most appropriate decision the function is created (Kulkarni and Lowe 2016). When the literature studies on the LC classification are examined, the radial basis function (RBF) of SVM is generally used in classifications and gives successful results (Knorn et al. 2009; Shi and Yang 2015; Noi and Kappas 2018). Therefore, we applied the RBF to classify the LC classes.

3.3. Artificial neural network

The ANN method, which is a machine learning algorithm in the field of artificial intelligence, is applied to determine the LC classes with satellite images. The ANN method composed of three layers involving the input, hidden and output layer (Kimes et al. 1998; Gomez et al. 2010; Xie et al. 2019). In this study, the input layer is spectral bands for each satellite image utilized for LC classification. The output layer is the number of LC classes and the hidden layer connects the components of the input layer and the output layer with a weighted channel. The important parameters of ANN involve the training threshold contribution, training rate, training root mean square error, training momentum, and the number of iterations. The training threshold contribution of 0.9000, the training rate of 0.2000, the training momentum rate of 0.9000 were applied. The training root mean square error was set to 0.1000. Furthermore, Many iterations (e.g. 100, 200, 500, and 1000) have been tried and the best result has been 1000 in this study. Therefore, it was used as 1000 in this study and then, the classification processes were applied. All the classifications were made in the ENVI software program.
In summary, the following satellite images were used to determine LC classes; (i) fused S1-VH and S1-VV with S2 satellite image (2), (ii) fused S1-VH and S1-VV with L8 satellite image (2), (iii) L8 MS bands and (iv) S2 MS bands.

3.4. Accuracy assessment

After classification processing according to three different classification approaches, the accuracy assessment of LC classification maps generated from different satellite images by using a stratified random sampling technique was applied to represent for each LC class. The accuracy assessment was carried out using 150 points depend on ground reference data (LC classes obtained from FCTM). Each point was checked on the ground reference data and classified images. Later, the accuracy of classification was calculated using error matrices (OA, KC, Producer's Accuracy (PA), and User's Accuracy (UA) for each LC class). Finally, the MLC, SVM, and ANN classification approach was applied to produce LC maps and the classification results (OA, KC, PA and UA) were compared with L8; S2 satellite images to assess the fusion data.

4. Results and Discussion

LC classification maps for six different satellite images (L8, L8-S1-VH, L8–S1-VV, S2, S2-S1-VH, and S2-S1-VV) were produced using MLC, SVM and ANN supervised classification techniques. Confusion matrices were produced for each classification technique to analyze class separation achievement for each classification technique with OA and KC assigned at Table 2-7 for MLC, SVM, and ANN, respectively. In comparison with the classification results depend on six different satellite images with MLC, SVM, and ANN classification techniques, the best OA of 96.67% and KC of 0.95 was obtained using MLC based on the combination of L8; S1-VV data. When the L8 satellite data alone were applied, the MLC provided the best OA of 92.00% and KC of 0.90 higher accuracy than SVM and ANN approaches (see Table 2). Contrary to, when the S2 satellite data alone were applied, the ANN provided the best OA of 89.92% and KC of 0.86 higher accuracy than MLC and SVM approach (see Table 3). Also, it was aimed to assess the role of S1-VH and S1-VV satellite images in improving LC classification OA and KC. The MLC, SVM, and ANN classification approaches were applied to the integrated S1-VH; S1-VV and, L8 and S2 satellite images. The use of the integrated images based on L8 and S2 data, and the S1-VH, S1-VV polarization data were acceptable results in classification accuracy. When the combined of L8 and S1-VH; S1-VV polarization data were used, the MLC provided the best OA of 93.33%

and 96.67%, and KC of 0.92 and 0.95 higher accuracy than the SVM and the ANN approaches, respectively (see Table 4 and 5). Furthermore, this result can be compared to the classification results of using L8 and S2 satellite images to assess the role of S1-VH; S1-VV satellite image in LC mapping. Therefore, the results of integrated satellite images were compared to those generated from in L8 and S2 data. Table 4 indicates that when S1-VH data with the fused L8 data, the classification accuracy increased with MLC approach applied. Also, such an integration decreased the classification accuracy when the SVM and ANN approaches was performed, in which an OA of 80.11% and 82.59%, and KC of 0.72 and 0.77 were achieved, respectively. Contrary to, the Table 5 shows when S1-VV data were incorporated into L8 data, the classification accuracy increased with MLC, SVM and ANN approaches were applied, in which an OA of 96.67%, 87.50%, and 86.72%, and KC of 0.95, 0.81 (not change for SVM) and 0.82 were achieved, respectively. Table 6 demonstrates that when S1-VH data was incorporated into S2 data, the classification accuracy was not changed by MLC, while SVM and ANN decreased. Table 7 displays that when S1-VV data were integrated into S2 data, the classification accuracy increased with MLC and SVM, while ANN decreased. Figure 3-4 indicates the results of LC classification using MLC, SVM, and ANN based on L8, S2, L8-S1-VH, L8-S1-VV, S2-S1-VH, and S2-S1-VV conducted with GIS. The PA and UA classification results are given in Table 2-7. The fused data with L8 and S1-VV satellite images using the MLC approach stands out with usually better results of the PA and UA (see Table 5). The worst PA and UA results were found for SVM and ANN approaches with the fused S2 and S1-VH data, respectively (see Table 6). The best results by class obtained from the CF class in the SVM approach that used the L8-S1-VV and S2-S1-VV data, where the results for PA were equal to 100% (see Table 5 and 7). Furthermore, the BF and MF classes in the MLC approach that utilized L8-S1-VV and S2-S1-VV data, where the results for PA were to equal to 100% (see Table 5 and 7). The best results by class were found for the BF classes in the ANN approach that used the L8-S1-VH data, where the results for UA were equal to 100% (see Table 7). Furthermore, the DF and other classes in the MLC approach that applied L8-S1-VV data, where the results for UA were equal to 100% (see Table 5). In addition, the MF classes in the SVM approach that performed S2-S1-VV data, where the results for UA were equal to 100% (see Table 7). The worst results by class were found for the DF class in the ANN approach that used the S2-S1-VH data, where the results for PA and UA were equal to 1.94% and 6.67%, respectively (see Table 7). However, the CF class achieved over 90% in PA for both all classification approaches and all satellite images used in this study (see Table 2-7). Also, the OA and KC related to different classification approaches and satellite images are shown in Figure 3 and 4 in this study. As can be seen in Figure 3 and 4, the best OA and KC values are obtained with the MLC method (except for the S2 satellite image). However, the SVM and ANN methods show a similar (except for fused S2-S1-VH) trend. Furthermore, the OA and kappa values were very close to each other in the classification performed on the fused L8-S1-VV data with SVM and ANN approaches.

Table 2. Comparison of accuracy assessment results with three classifiers based on L8 data.

LC Classes	MLC		SVM		ANN	
	PA	UA	PA	UA	PA	UA
CF	96.55%	93.33%	100%	84.17%	98.68%	97.54%
BF	96.43%	90.00%	60.78%	77.18%	85.84%	52.72%
MF	90.00%	90.00%	74.84%	88.38%	51.66%	94.39%
DF	85.29%	96.67%	95.56%	87.76%	62.63%	87.32%
Other	93.10%	90.00%	94.62%	84.89%	94.75%	81.00%
OA	92.00%		85.05%		83.57%	
KC	0.90		0.81		0.78	

Table 3. Comparison of accuracy assessment results with three classifiers based on S2 data.

LC Classes	MLC		SVM		ANN	
	PA	UA	PA	UA	PA	UA
CF	90.32%	93.33%	98.93%	93.73%	97.26%	99.30%
BF	92.59%	83.33%	16.15%	82.35%	20.77%	61.36%
MF	78.13%	83.33%	95.42%	86.76%	98.75%	88.60%
DF	81.25%	86.67%	52.97%	93.70%	68.17%	91.99%
Other	85.71%	80.00%	91.61%	80.29%	91.30%	82.88%
OA	85.33%		87.59%		89.92%	
KC	0.82		0.82		0.86	

Table 4. Comparison of accuracy assessment results with three classifiers based on fused L8 and S1- VH data.

LC Classes	MLC		SVM		ANN	
	PA	UA	PA	UA	PA	UA
CF	93.10%	90.00%	91.41%	71.19%	93.57%	82.91%
BF	87.88%	96.67%	35.17%	45.26%	13.67%	100.00%
MF	96.67%	96.67%	96.73%	91.44%	96.79%	88.06%
DF	96.43%	90.00%	36.71%	53.90%	82.64%	67.45%
Other	93.33%	93.33%	91.53%	78.36%	86.30%	83.81%
OA	93.33%		80.11%		82.59%	
KC	0.92		0.72		0.77	

Table 5. Comparison of accuracy assessment results with three classifiers based on fused L8 and S1-VV data.

LC Classes	MLC		SVM		ANN	
	PA	UA	PA	UA	PA	UA
CF	93.55%	96.67%	100%	90.55%	99.76%	95.94%
BF	100.00%	90.00%	83.36%	89.94%	47.39%	90.37%
MF	96.67%	96.67%	82.54%	85.29%	94.92%	87.25%
DF	93.75%	100.00%	21.01%	27.17%	68.23%	69.07%
Other	100.00%	100.00%	80.68%	86.91%	89.67%	75.06%
OA	96.67%		87.50%		86.72%	
KC	0.95		0.81		0.82	

Table 6. Comparison of accuracy assessment results with three classifiers based on fused S2-S1-VH data.

LC Classes	MLC		SVM		ANN	
	PA	UA	PA	UA	PA	UA
CF	96.43%	90.00%	99.40%	88.40%	100.00%	90.81%
BF	93.33%	93.33%	42.93%	97.24%	2.04%	76.19%
MF	93.55%	96.67%	79.81%	86.87%	100.00%	66.50%
DF	90.63%	96.67%	93.03%	63.94%	1.94%	6.67%
Other	96.55%	93.33%	60.97%	48.38%	97.57%	58.33%
OA	85.33%		87.37%		76.82%	
KC	0.82		0.82		0.66	

Table 7. Comparison of accuracy assessment results with three classifiers based on fused S2-S1-VV data.

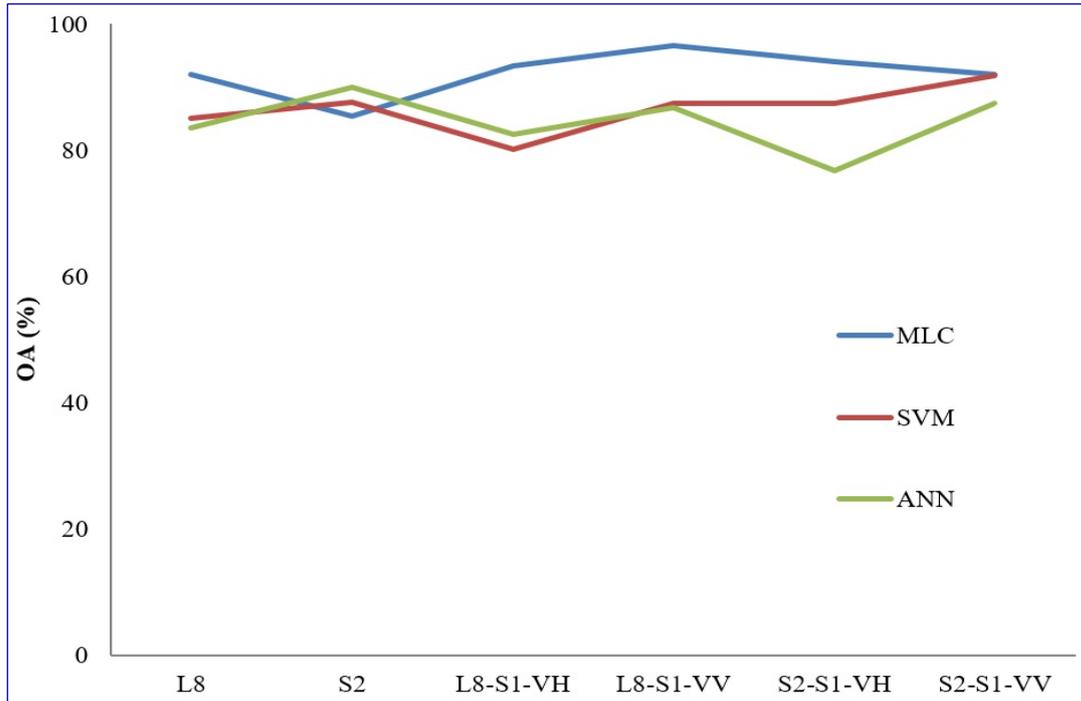| LC Classes	MLC		SVM		ANN	
	PA	UA	PA	UA	PA	UA
CF	90.63%	96.67%	100.00%	93.77%	100.00%	85.42%
BF	82.35%	93.33%	54.59%	96.03%	49.37%	94.24%
MF	100.00%	83.33%	100.00%	100.00%	99.73%	93.33%
DF	93.55%	96.67%	85.75	85.12%	96.88%	74.04%
Other	96.43%	90.00%	100.00%	83.24%	74.48%	95.33%
OA	92.00%		91.93%		87.51%	
KC	0.90		0.90		0.84	

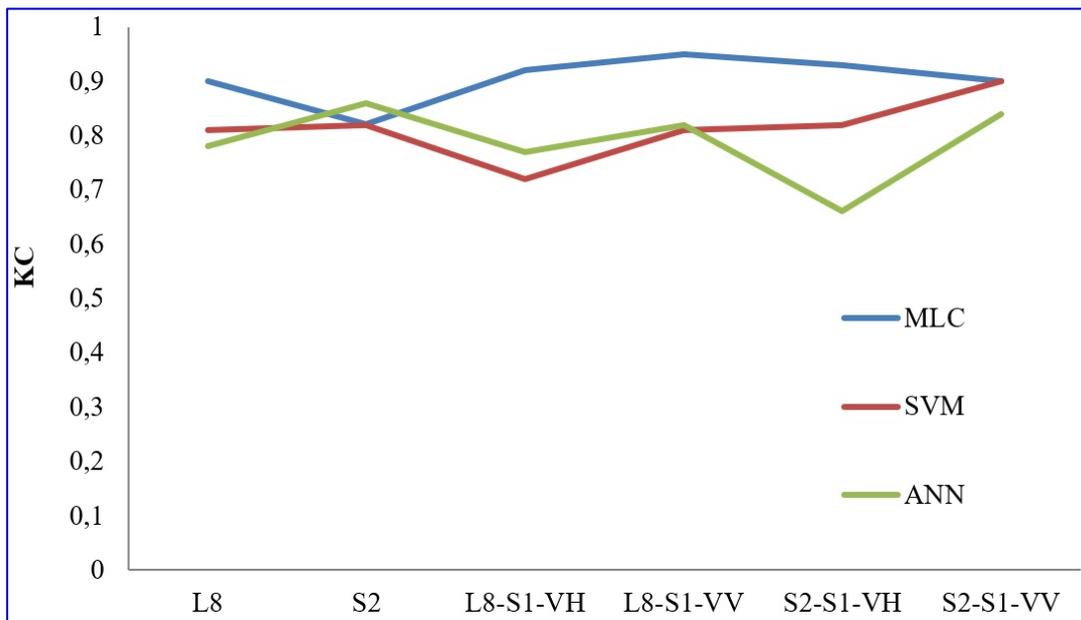Figure 3. The change of OA according to the MLC, SVM and ANN with satellite images.

Figure 4. The change of KC according to the MLC, SVM and ANN with satellite images.

The classification successes for determining LC classes were determined by using three different classification approaches (MLC, SVM, and ANN) and six different remote sensing data (L8, L8; S1-VH, L8; S1-VV, S2, S2; S1-VH and S2; S1-VV) in our study. According to the classification approaches, the MLC obtained better LC classification results than those of the SVM and ANN for the fused data L8; S1-VH and L8; S1-VV. The integration of L8 and S1-VH and S1-VV satellite data using MLC approach increases the overall classification accuracy. This is similar result obtained from previous research (Lu et al., 2012; Lu et al., 2014; Sameen et al., 2016). When the studies on the subject are examined in the literature, although many classification approaches are used to determine LC classes, it is not clear which classification approach gives the best results. In some studies, as in our study the MLC (Lu et al., 2012; Morgan et al., 2015), in some SVM (Dixon and Candade 2008; Şerifoğlu Yılmaz et al., 2018, Noi and Kappas, 2018), and some ANN (Szuster et al., 2011; Srivastava et al., 2012; Verma et al., 2020) the best classification success was achieved. However, when many studies are

examined, the classification successes obtained from different satellite images such as Landsat 7 ETM+ (Günlü et al., 2008), Landsat 5 TM and Spot (Lu et al., 2012), Landsat ETM+ and OLI (Jia et al., 2014), Hyperion (Elatawneh et al., 2014), L8 and S2 (Topaloglu et al., 2016), WorldView-2 (Şerifoğlu Yılmaz et al., 2018), Aster and Hyperion (Mann and Joshi, 2017), S2 (Steinhausen et al. 2018), Rapideye (Sirro et al. 2018) and ZiYuan (ZY-3) (Xie et al., 2019) used in determining LC classes also differ. However, in the literature studies examined, there are some studies carried out to determine LC classes by using passive and active satellite images together in recent years. It is stated that using the data set obtained by evaluating the active and passive remote sensing data together, the classification success of the LC classes generally increases (Hyde et al., 2006; Erasmi and Twele 2009; Bagan et al., 2012; Van Beijma et al., 2014; Clerici et al., 2017). In many studies conducted as in our study to support the above-mentioned statement, it was observed that the classification success increased by using the active and passive satellite images together. This is in line with the findings in other LC classification studies in different geographic regions that fused optical and radar data satellite systems (Soria-Ruiz et al., 2010; Lu et al., 2012; Deus, 2016; Sameen et al., 2016; Steinhausen et al., 2018; Muthukumarasamy et al., 2019, Tavares et al., 2019). However, classification successes for fused data vary according to the classification method used. For example, the MLC approach achieved better LC classes results in our study. In contrast to the MLC approach, in some studies, the SVM (Zakeri et al., 2017; Clerici et al., 2017; Zhang and Xu, 2018; Xie et al., 2019) and in other studies, the ANN (Pacifici et al., 2008; Kussul et al., 2016) approach gave better results. The classification accuracy assessment (OA and KC) has been applied for both passive satellite data, and passive and active satellite data are evaluated together by using MLC, SVM and ANN approach. For only L8 satellite image, the MLC (92.00% - 0.90) provided the best results classification accuracy compared to SVM (85.05% -0.81) and ANN (83.57% - 0.78). For the combination of L8 and S1-VH and S1-VV data, the MLC (93.33% - 0.92; 96.67% - 0.95) has higher classification accuracy compared to SVM (80.11% - 0.72; 87.50% - 0.81) and ANN (82.59% - 0.77; 86.72% - 0.82), respectively. For only S2 data, the ANN (89.92% - 0.86) slightly improved classification accuracy compared to SVM (87.59% - 0.82) and MLC (85.33% - 0.82). For the integration of S2 and S1-VH data, the SVM (87.37% - 0.82) slightly increased classification accuracy compared to MLC (85.33% - 0.82) and ANN (76.82% - 0.66). In contrast, for the fused S2 and S1-VV data, the the MLC (92.00% - 0.90) slightly increased classification accuracy compared to SVM (91.93% - 0.90) and higher classification accuracy compared to ANN (87.51% - 0.84). In general, for the fused data the non-parametric approaches have poorer performance than MLC. Separability values of LC classes using the integrated of L8; S2 and S1-VH and S1-VV (except for S2; S1-VH) satellite data are higher compared to L8 and S2 satellite image. It was seen that the OA and KC with fused image (L8; S1-VV) with MLC were improved by 5.1 and 5.6%, respectively, compared with the only L8 data. Similarly, the OA and KC with fused image (S2; S1-VV) with MLC were increased by 2.3% and 5.6%, respectively, compared with the only S2 data. Many investigations indicate that using these fused data together in LC classification processing would give higher accuracy as compared to individual data classification results. Comparing the results from the OA and KC with other studies indicates that ALOS PALSAR and Landsat 5 TM data were applied by Lu et al., (2014) to classify LC classes using MLC, ANN and SVM approach. The fusion of Landsat 5 TM and ALOS PALSAR satellite data using MLC provides better classification than individual sensor data. Similar to our study were attained by Clerici et al., (2017) mapped LC classes using S1 and S2 data with SVM, and concluded that the fused data is more better classification accuracy than the individual data. Their study results reported that the combination of S1 and S2 data using SVM was used to classify LC classes with the OA of 88.75% and a KC of 0.86, whereby the SVM had an OA of 72.5% and a KC of 0.67 when only S2 was used to classify LC classes. Classification accuracy increased when Sukawattanavijit and Chen (2015) conducted the integrated of Radarsat-2 and L8 imagery using the SVM provides better accuracy than the MLC. Deus (2016) integrated the Landsat 5 TM and ALOS PALSAR L band data using an SVM approach to classify LC classification, which achieved an OA of 95%. Although the OA obtained in this study was similar to our study, however, the method used varied. Similar results were obtained by Abdikan (2018) fused the Landsat TM and ALOS PALSAR data using only the SVM approach to map LC classification in forest areas, Turkey, which obtained an OA of 94.316% and KC of 0.924. Muthukumarasamy et al., (2019) who applied the use of SVM was achieved with integration of LISS-IV and S1 with OA and KC of 92%, 0.81, respectively. Also, Zhang and Xu (2018) applied the fused data with MLC, SVM and ANN approaches. Their study results demonstrated that the best value for the SVM classification, whereas the fused data increased the accuracy by 10%. Adding S1-VH and S1-VV polarization contributed to increase the classification accuracy of integrated the S2 data in our study, which was a similar result observed by Khan et al., (2020). They combined the S1-VH polarization fused with the S2 image had a high classification accuracy of 85% compared to 84% accuracy for S1-VV-polarization fused with S2 data.

In this study, eighteen different LC class maps using three different classification methods, and six different satellite images were produced. As mentioned before, in the production of these maps, the LC classes map (Figure 2) generated from FCTM was used as ground data. LC classes maps (Figure 5-7) obtained using classification methods and satellite images were compared with LC classes map obtained from FCTM. As a

result of the comparison, it was found that the maps produced by using the L8-S1-VH-VV (Figure 5 b and c) and S2-S1-VH-VV (Figure 5 e and f) satellite images with MLC are more consistent with the map of LC classes (Figure 2) produced from the FCTM. However, LC classes in L8-S1-VH and VV (especially VV) using the MLC have shown that LC classes are more prominent than LC classes obtained by using the S2-S1-VH and VV with MLC (Figure 5). It is seen that the areas shown in yellow color in the south of the study area and expressed as other areas are more accurately determined in the L8-S1-VV image (Figure 5c). However, in other images (L8-S1-VH, S2-S1-VH and S2-S1-VV), this area was mixed with other classes (Figure 6 b, e and f). As seen in Figure 8-9, it is seen that the level of success of PA and UA for each class is over 80% in all satellite images using the MLC method.
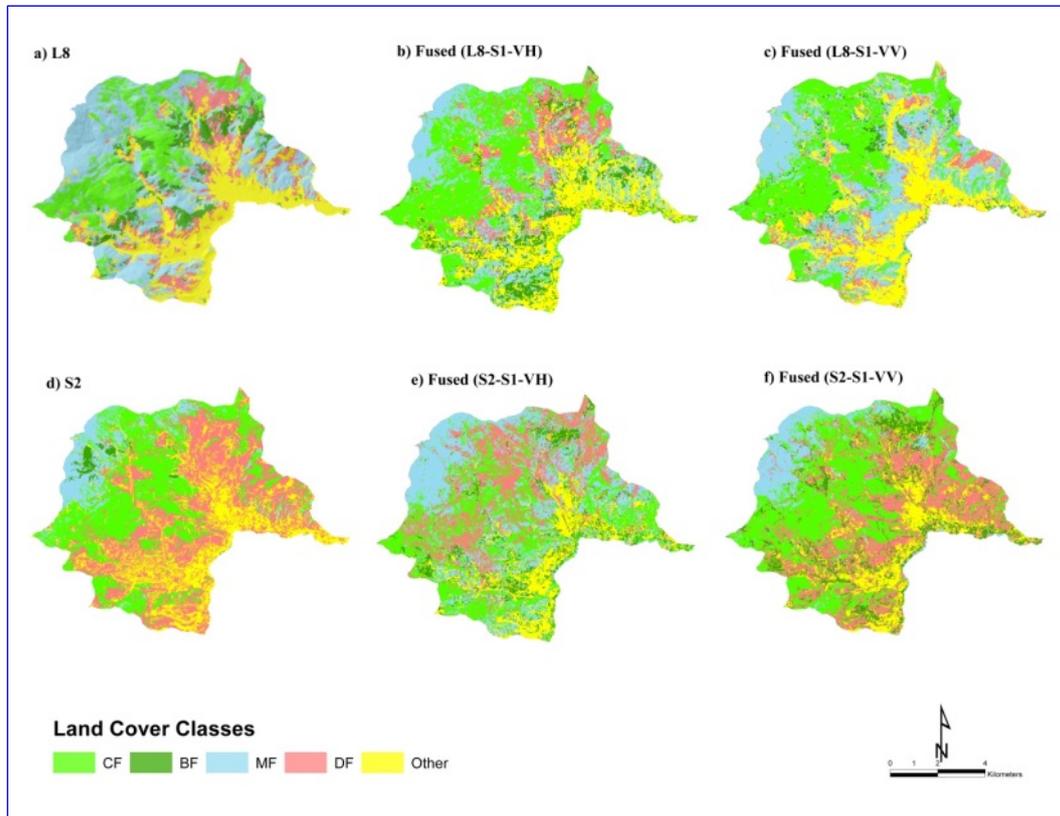

Figure 5. Comparison of the MLC approach: a) only L8 MS b) L8-S1-VH fused c) L8-S1-VV fused d) only S2 MS e) S2-S1-VH fused f) S2-S1-VV fused.
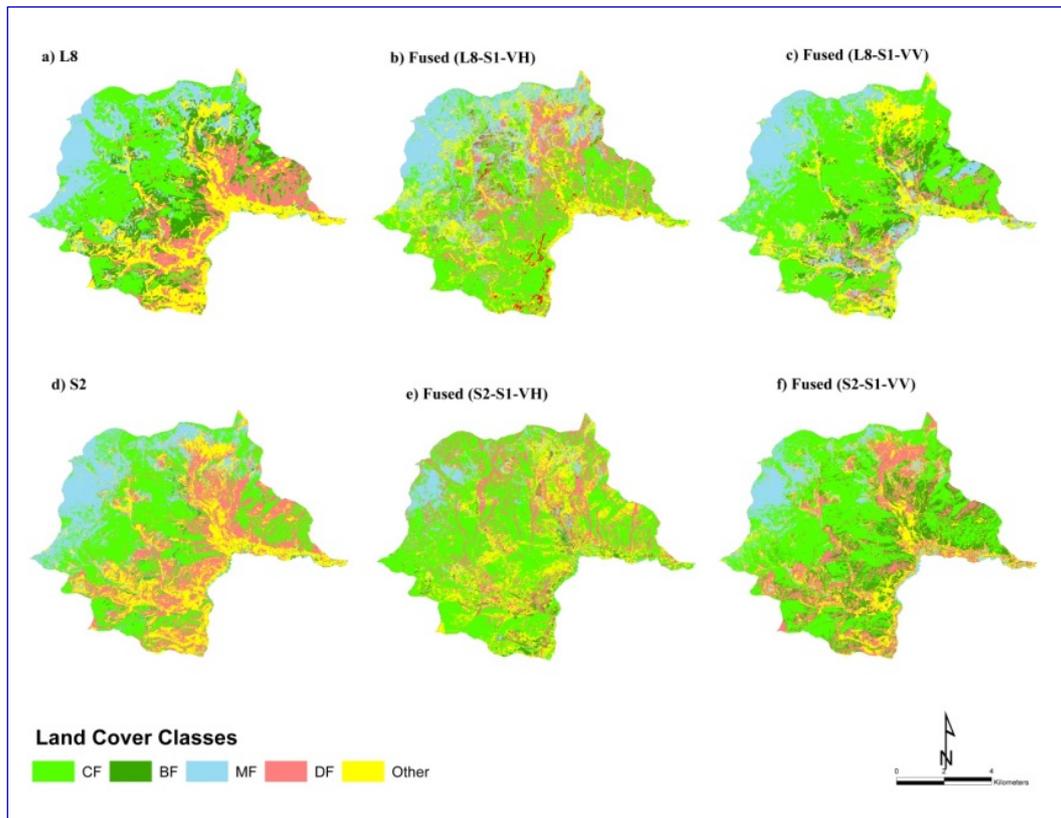
Figure 6. Comparison of the SVM approach: a) only L8 MS b) L8-S1-VH fused c) L8-S1-VV fused d) only S2 MS e) S2-S1-VH fused f) S2-S1-VV fused.
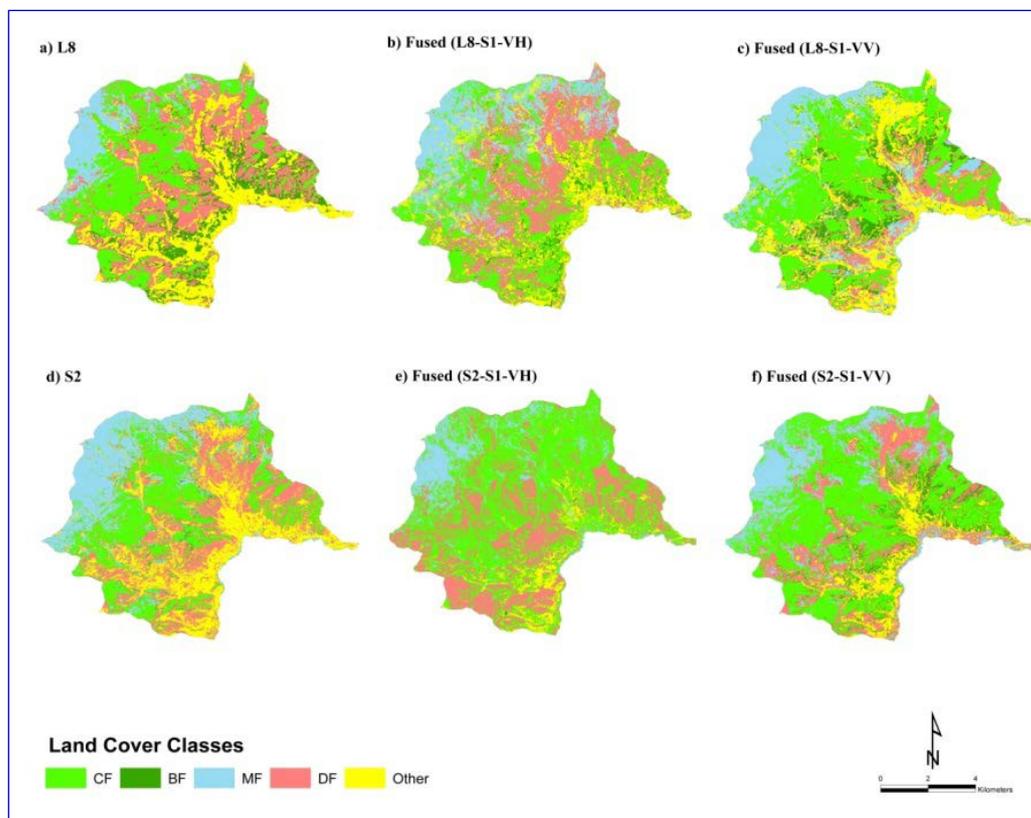

Figure 7. Comparison of the ANN approach: a) only L8 MS b) L8-S1-VH fused c) L8-S1-VV fused d) only S2 MS e) S2-S1-VH fused f) S2-S1-VV fused.
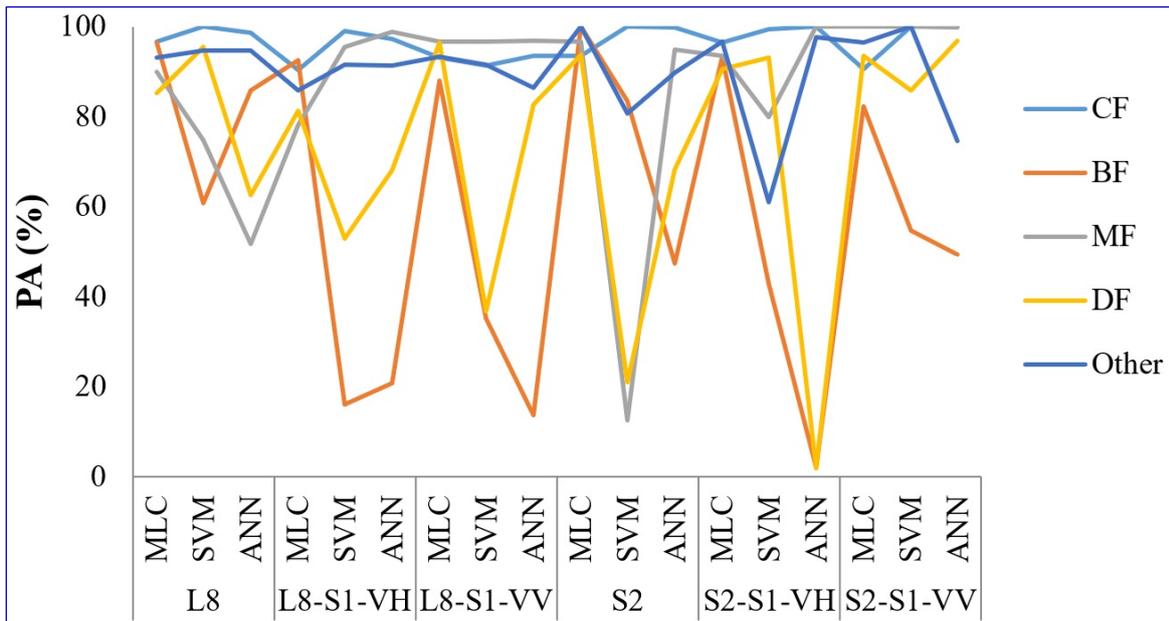
Figure 8. The change of PA according to the MLC, SVM and ANN with satellite images.
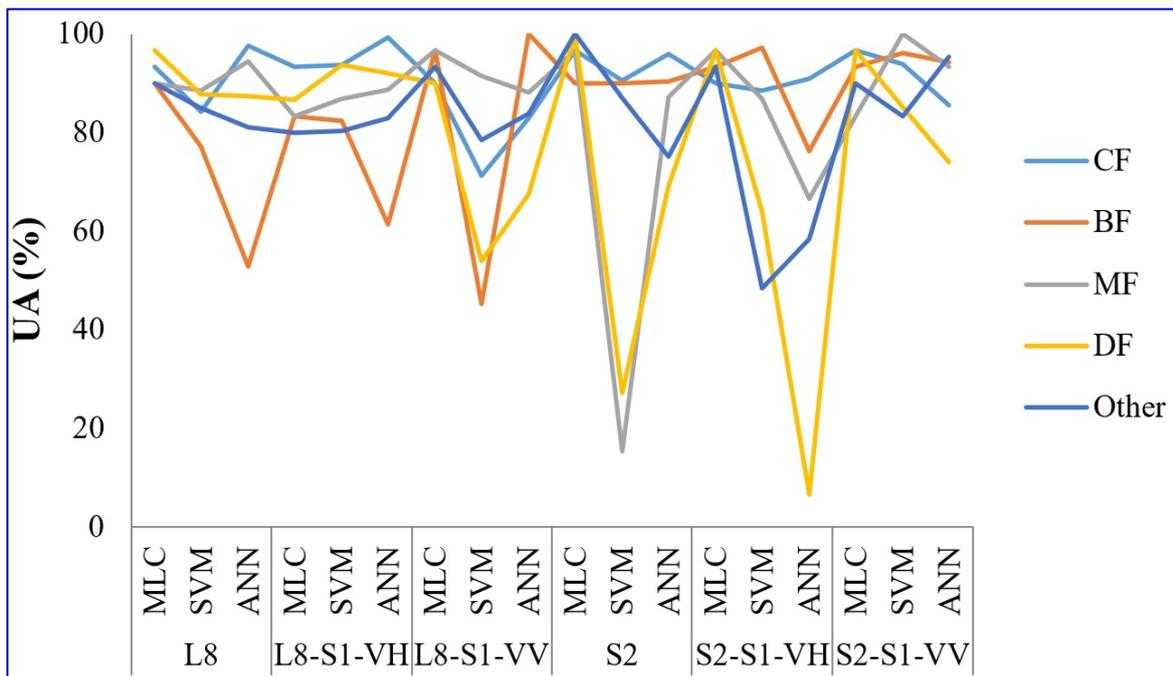

Figure 9. The change of UA according to the MLC, SVM and ANN with satellite images.

On the other hand, it was observed that the success levels of all satellite images using SVM and ANN methods varied. The difference in the classification results between the MLC, SVM and ANN classifiers was that the LC classes in other class regions were misclassified using the SVM and ANN classifier. It has been observed that PA and UA accuracy, especially for BF and DF classes, are low in some satellite images using SVM and ANN. The reasons for this can be explained as follows; the heterogeneous structure of LC classes other than CF and MF can be effective in the study area. As a result, especially in the classification processing, the DF class was misclassified because it has similar reflectance values with the areas expressed as other classes. The DF, BF, and other classes were confused because they may have similar reflectance. Moreover, some LC classes such as MF and BF can also be easily confused as they have similar reflectance signals. Similar results were obtained from studies by (Waser et al. 2011). This study and other studies in the literature on the subject indicated that the accuracy levels obtained in determining LC classes vary based on the satellite image used, classification

technique, land structure, the structure of stands in the study area and LC classes have similar characteristics, etc. Therefore, it is seen that there is no prescription to determine the best success in determining LC classes.

5. Conclusions

In order to determine LC classes, the classification accuracy assessment was evaluated and compared for both optical (L8, S2) and fusion (S1-VH-L8; S1-VV-L8; S1-VH-S2; S1-VV-S2) data by using MLC, SVM and ANN approaches. Differences between the classification successes were found when using satellite data and classification approaches. Generally, the MLC approach outperformed the SVM and ANN when classifying various LC classes using the optical and fusion data. The study also indicated that S1-VH and S1-VV data can increase the OA and KC of LC classes classification when combined with L8 and S2, particularly when the L8 data and MLC is applied. Furthermore, the combination of L8; S2, and S1-VH and S1-VV data generated features decreased the spectral confusion between some LC classses. However, while the fusion of the L8; S2 and, S1-VH; S1-VV data classification accuracy was increased, the classification accuracy for some LC classes was still lower than that of the optical data. In the future investigations using different classification approaches such as object-oriented and deep learning classification with high resolution active and passive satellite data, especially in mixed forest ecosystems, can be carried out to assess their potential in LC classes and mapping. In addition, it may increase the success levels of LC classes.

Acknowledgments

References

1. **Abdikan, S. (2018).** Exploring image fusion of ALOS/PALSAR data and Landsat data to differentiate forest area. *Geocarto International*, 33(1), 21-37.
2. **Anonymous (2018).** Ankara Regional Directorate of Forestry, Eskipazar Forest Managemet Enterprise, Ören Forest managemet planning unit ecosystem based multiple use forest management planning. P:247.
3. **Bagan, H., Kinoshita, T., Yamagata, Y. (2012).** Combination of AVNIR-2, PALSAR, and polarimetric parameters for land cover classification. *IEEE Transactions on Geoscience and Remote Sensing*, 50(4), 1318–1328.
4. **Ban, Y., Peng, G., Giri, C. (2015).** Global land cover mapping using Earth observation satellite data: Recent progresses and challenges. *ISPRS Journal of Photogrammetry and Remote Sensing*, 10.1016/j.isprsjprs.2015.01.001.
5. **Bulut, S., Günlü, A. (2016).** Comparison of different supervised classification algorithms for land use classes. Kastamonu University, Journal of Forestry Faculty, 16 (2), 528-535.
6. Burkhard, B., Kroll, F., Nedkov, S., Müller, F. (2012). Mapping ecosystem service supply, demand and budgets. Ecol. Indic. 21, 17–29.
7. **Büyüksalih, İ. (2016).** Landsat images classification and change analysis of land cover/use in Istanbul. *International Journal of Environment and Geoinformatics*, 3(2), 56-65.
8. **Camargo, F.F., Sano, E.E., Almedia, M., Mura, J.C., Almedia, T. (2019).** A Comparative assessment of machine-learning techniques for land use and land cover classification of the Brazilian Tropical Savanna using ALOS-2/PALSAR-2 polarimetric images. *Remote Sensing*, 11, 1600.
9. **Clerici, N., Calderon, C.A.V., Posada, J.M. (2017).** Fusion of Sentinel-1A and Sentinel-2A data for land cover mapping: a case study in the lower Magdalena region, Colombia. *Journal of Maps*, 13(2), 718–726.
10. **Deus, D. (2016).** Integration of ALOS PALSAR and Landsat data for land cover and forest mapping in Northern Tanzania. *Land,* 5, 43.
11. **Dixon, B., Candade, N. (2008).** Multispectral landuse classification using neural networks and support vector machines: one or the other, or both? *International Journal of Remote Sensing*, 29(4), 1185-1206.
12. **Elatawneh, A., Kalaitzidis, C., Petropoulos, G.P., Schneider, T. (2014).** Evaluation of diverse classification approaches for land use/cover mapping in a mediterranean region utilizing hyperion data. *International Journal of Digital Earth*, 7(3),194–216.

13. **Erasmi, S., Twele, A. (2009).** Regional land over mapping in the humid tropics using combined optical and SAR satellite data – a case study from Central Sulawesi, Indonesia. *International Journal of Remote Sensing*, 30, (10), 2465–2478.

14. **Fonteh, M.L., Theophile, F., Cornelius, M.L., Main, R., Ramoelo, A., Cho, M.A. (2016).** Assessing the utility of Sentinel-1 C band synthetic aperture radar imagery for land use land cover classification in a tropical coastal systems when compared with Landsat 8. *Journal of Geographic Information System*, 8, 495-505.

15. **Fry, J.A., Xian, G., Jin, S., Dewitz, J.A., Homer, C.G., Yang, L., Barnes, C.A., Herold, N.D., Wickham, J.D. (2012).** Completion of the 2006 national land cover database for the conterminous United States. *Photogramm. Eng. Remote Sens.*, 77, 858–864.

16. **Gebhardt, S., Wehrmann, T., Ruiz, M.A.M., Maeda, P., Bishop, J., Schramm, M., Kopeinig, R., Cartus, O., Kellndorfer, J., Ressl, R., Santos, L.A., Schmidt, M. (2014).** MAD-MEX: Automatic wall-to-wall land cover monitoring for the Mexican REDD-MRV program using all Landsat data. *Remote Sens.*, 6, 3923-3943.

17. **Gomez, C., Mangeas, M., Petit, M., Corbane, C., Hamon, P. (2010).** Use of high-resolution satellite imagery in an integrated model to predict the distribution of shade coffee tree hybrid zones. *Remote Sens. Environ.*, 114, 2731–2744.

18. **Guidici, D., Clark, M.L. (2017).** One-dimensional convolutional neural network land-cover classification of multi-seasonal hyperspectral imagery in the San Francisco Bay area, California. *Remote Sens.*, 9, 629.

19. **Günlü, A., Sivrikaya, F., Başkent, E.Z., Keleş, S., Çakır, G., Kadıoğulları, A.İ. (2008).** Estimation of stand type parameters and land cover using Landsat-7 ETM image: a case study from Turkey. *Sensors*, 8, 2509-2525.

20. **Han, N., Wang, K., Yu, L., Zhang, X. (2012).** Integration of texture and landscape features into object-based classification for delineating Torreya using IKONOS imagery. *Int. J. Remote Sens.*, 33(7), 2003–2033.

21. **Hong, G., Zhang, A., Zhou, F., Brisco, B. (2014).** Integration of optical and synthetic aperture radar (SAR) images to differentiate grassland and alfalfa in Prairie area. *Int. J. Appl. Earth Obs. Geoinf.*, 28 (1), 12–19.

22. **Hussain, S., Mubeen, M., Ahmad, A., Akram, W., Hammad, H.M., Ali, M., Masood, N., Amin, A., Farid, H.U., Sultana, S.R., Fahad, S., Wang, D., Nasim, W. (2020).** Using GIS tools to detect the land use/land cover changes during forty years in Lodhran district of Pakistan. *Environmental Science and Pollution Research*, https://doi.org/10.1007/s11356-019-06072-3.

23. **Hütt, C., Koppe, W., Miao, Y., Bareth, G. (2016).** Best accuracy Land use/Land cover (LULC) classification to derive crop types using multitemporal, multisensor, and multi-polarization SAR satellite images. *Remote Sens.*, 8, 684.

24. **Hyde, P., Dubayah, R., Walker, W., Blair, J.B., Hofton, M., Hunsaker, C. (2006).** Mapping forest structure for wildlife habitat analysis using multi-sensor (LiDAR, SAR/inSAR, ETM+, QuickBird) synergy. *Remote Sens. Environ.*, 102, 63–73.

25. **Jia, K., Wu, B.F., Tian, Y.C., Zeng, Y., Li, Q.Z. (2011).** Vegetation classification method with biochemical composition estimated from remote sensing data. *Int J Remote Sens.*, 32(24), 9307–9325.

26. **Jia, K., Wei, X., Gu, X., Yao, Y., Xie, X., Li, B. (2014).** Land cover classification using Landsat 8 operational land imager data in Beijing, China. *Geocarto International*, 29 (8), 941–951.

27. **Juliev, M., Pulatov, A., Fuchs, S., Hübl, J. (2019).** Analysis of land use land cover change detection of Bostanlik District, Uzbekistan. *Pol. J. Environ. Stud.*, 28(5), 3235-3242.

28. **Khan, A., Govil, H., Kumar, G., Dave, R. (2020).** Synergistic use of Sentinel-1 and Sentinel-2 for improved LULC mapping with special reference to bad land class: a case study for Yamuna River floodplain, India. *Spat. Inf. Res.*, https://doi.org/10.1007/s41324-020-00325-x.

29. **Khatami, R., Mountrakis, G., Stehman, S.V.A. (2016).** Meta-analysis of remote sensing research on supervised pixel-based land cover image classification processes: General guidelines for practitioners and future research. *Remote Sens. Environ.*, 177, 89–100.

30. **Kimes, D.S., Nelson, R.F., Manry, M.T., Fung, A.K. (1998).** Attributes of neural networks for extracting continuous vegetation variables from optical and radar measurements. *Int. J. Remote Sens.*, 19, 2639–2663.

31. **Knorn, J., Rabe, A., Radeloff, V.C., Kuemmerle, T., Kozak, J., Hostert, P. (2009).** Land cover mapping of large areas using chain classification of neighboring Landsat satellite images. *Remote. Sens. Environ.*, 113, 957–964.

32. **Kuemmerle, T., Erb, K., Meyfroidt, P., Müller, D., Verburg, P. H., Estel, S., Reenberg, A. (2013).** Challenges and opportunities in mapping land use intensity globally. Current Opinion in Environmental *Sustainability*, 5(5), 484–493.

33. **Kulkarni, A.D., Lowe B. (2016).** Random forest algorithm for land cover classification. *International Journal on Recent and Innovation Trends in Computing and Communication*, 4(3), 58-63.

34. **Kussul, N., Lemoine, G., Gallego, F.J., Skakun, S.V., Lavreniuk, M., Shelestov, A.Y. (2016).** Parcel-based crop classification in Ukraine using Landsat-8 data and Sentinel-1A data. *IEEE Journal of Selected Topics in Applied Earth Observations and Remote Sensing*, 9(6), 2500–2508.

35. **Lillesand, T., Kiefer, R., Chipman, J. (2004).** Remote Sensing and Image Interpretation. 5th Edn., John Wiley and Sons, New York, USA.

36. **Lu, D., Weng, Q. A. (2007).** Survey of image classification methods and techniques for improving classification performance. *International Journal of Remote Sensing*, 28, 823-870.

37. **Lu, D., Batistella, M., Li, G., Moran, E., Hetrick, S., Freitas, C.D.C., Futra, L.V., Anna, J.S.S. (2012).** Land use/cover classification in the Brazilian Amazon using satellite images. *Brasília*, 47(9), 1185-1208.

38. **Lu, D., Li, G., Moran, E., Kuang, W. (2014).** A comparative analysis of approaches for successional vegetation classification in the Brazilian Amazon. *GIScience & Remote Sensing*, 51(6), 695–709.

39. **Mann, D., Joshi, P.K. (2017).** Evaluation of image classification algorithms on hyperion and aster data for land cover classification. *Proceedings of the National Academy of Sciences*, India - Section A 87(1). https://doi.org/10.1007/s40010-017-0454-6.

40. **Miettinen, J., Liew, S.C. (2011).** Separability of insular South east Asian woody plantation species in the 50 m resolution Alos Palsar mosaic product. *Remote Sensing Letters*, 2, 299–307.

41. **Mohajane, M., Essahlaoui, A., Oudija, F., Hafyani, M.E., Hmaidi, A.E., Ouali, A.E., Randazzo, G., Teodora, C. (2018).** Land use/Land cover (LULC) using Landsat data series (MSS, TM, ETM+ and OLI) in Azrou Forest, in the Central Middle Atlas of Morocco. *Environments*, 5, 131.

42. **Morgan, R.S., Rahim, I.S., El-Hady, M.A. (2015).** A Comparison of classification techniques for the land use/ land cover classification. *Global Advanced Research Journal of Agricultural Science*, 4(11), 810-818.

43. **Mountrakis, G., Im, J., Ogole, C. (2011).** Support vector machines in remote sensing: a review. *ISPRS J Photogramm Remote Sens* 66:247–259

44. **Mushore, T.D., Mutanga, O., Odindi, J., Dube, T. (2017).** Assessing the potential of integrated Landsat 8 thermal bands, with the traditional reflective bands and derived vegetation indices in classifying urban landscapes. *Geocarto InternatIonal*, 32(8), 886–899.

45. **Muthukumarasamy, I., Shanmugam, R.S., Usha, T. (2019).** Incorporation of textural information with SAR and optical imagery for improved land cover mapping. *Environmental Earth Sciences*, 78, 643.

46. **Noi, P.T, Kappas M. (2018).** Comparison of random forest, k-nearest neighbor, and support vector machine classifiers for land cover classification using Sentinel-2 imagery. *Sensors*, 18, 18.

47. **Pacifici, F., Frate, F.D., Emery, W.J., Gamba, P., Chanossot, J. (2008).** Urban mapping using coarse sar and optical data: outcome of the 2007 GRSS Data Fusion Contest. *IEEE Geoscıence And Remote Sensıng Letters*, 5(3), 331-335.

48. **Pal, M., Mather, P. M. (2004).** Assessment of the effectiveness of support vector machines for hyperspectral data. *Future Generation Computer Systems*, 20(7), 1215-1225.

49. **Pradhan, R., Pradhan, M.P., Bhusan, A., Pradhan, R.K., Ghose, M.K. (2010).** Land-cover classification and mapping for eastern Himalayan State Sikkim. *Journal of Computing*, 2(3), 166-170.

50. **Rao, K.V.R., Kumar, R. (2017).** Land cover classification using Sentinel-1 SAR data. International *Journal for Research in Applied Science & Engineering Technology*. 5(12), 1054-1060.

51. **Ridwan, I., Bisri, M., Yusran, F.H., Hakim, L., Kadir, S. (2017).** Identification of characteristics of land cover in mangkauk catchment area Using support vector machine (SVM) and artificial neural network (ANN). *American Journal of Applied Sciences*, 14 (7), 726-736.

52. **Sameen, M.I., Nahhas, F.H., Buraihi, F.H., Pradhan, B., Shariff, A.R.B.M. (2016).** A refined classification approach by integrating Landsat Operational Land Imager (OLI) and Radarsat-2 imagery for land-use and land-cover mapping in a tropical area. *Internatıonal Journal of Remote Sensıng*, 37(10), 2358–2375.

53. **Shi D., Yang X. (2015).** Support vector machines for land cover mapping from remote sensor imagery. In: Li J., Yang X. (eds) Monitoring and Modeling of Global Changes: A Geomatics Perspective. Springer Remote Sensing/Photogrammetry. Springer, Dordrecht. https://doi.org/10.1007/978-94-017-9813-6_13

54. **Shivakumar, B.R., Rajashekararadhya, S.V. (2018).** Investigation on land cover mapping capability of maximum likelihood classifier: a case study on North Canara, India. *Procedia Computer Science*, 143, 579–586.

55. **Sirro, L., Häme, T., Rauste, Y., Kilpi, J., Hämäläinen, J., Gunia, K., Jong, B.D., Pellat, F.P. (2018).** Potential of different optical and SAR data in forest and land cover classification to support REDD+ MRV. *Remote Sens.*, 10, 942.

56. **Soria-Ruiz, J., Fernandez-Ordonez, Y., Woodhouse, L. (2010).** Land-cover classification using radar and optical images: a case study in Central Mexico. *International Journal of Remote Sensing*, 31(2), 3291-3305.

57. **Srivastava, P.K., Han, D., Rico-Ramirez, M.A., Bray, M., Islam, T. (2012).** Selection of classification techniques for land use/land cover change investigation. *Advances in Space Research*, 50, 1250–1265.

58. **Steinhausen, M., Wagner, P.D., Narasimhan, B., Waske, B. (2018).** Combining Sentinel-1 and Sentinel-2 data for improved land use and land cover mapping of monsoon regions. *International Journal of Applied Earth Observation and Geoinformation*, 73, 595-604

59. **Sukawattanavijit, C., Chen J. (2015).** Fusion of Radarsat-2 imagery with Landsat-8 multispectral data for improving land cover classification performance using SVM. *IEEE 5th Asia-Pacific Conference on Synthetic Aperture Radar (APSAR)*, Singapore, pp. 567-572.

60. **Szuster, B.W., Chen, Q., Borger, M. (2011).** A comparison of classification techniques to support land cover and land use analysis in tropical coastal zones. *Applied Geography*, 31, 525-532.

61. **Şerifoğlu Yılmaz, Ç., Güngör, O., Kahraman, H.T. (2018).** Land cover mapping with advanced classification algorithms, *Nature Sciences* (NWSANS), 13(3), 41-50.

62. **Tavares, P.A., Beltrão, N.E.S., Guimarães, U.S., Teodoro, A.C. (2019).** Integration of Sentinel-1 and Sentinel-2 for classification and LULC mapping in the urban area of Belém, Eastern Brazilian Amazon. *Sensors*, 19, 1140.

63. **Topaloglu, H.R., Sertel, E., Musaoglu, N. (2016).** Assessment of classification accuracies of Sentinel-2 and Landsat-8 data for land cover/use mapping. *In International Archives of the Photogrammetry, Remote Sensing and Spatial Information Sciences; ISPRS*: Prague, Czech Republic, Volume XLI-B8, pp. 1055–1059.

64. **Ullah, S., Tahir, A.A., Akbar, T.A., Hassan, Q.K., Dewan, A., Khan, A.J., Khan, M. (2019).** Remote sensing-based quantification of the relationships between land use land cover changes and surface temperature over the lower Himalayan region. *Sustainability*, 11, 5492.

65. **Van-Beijma, S., Comber, A., Lamb, A. (2014).** Random forest classification of salt marsh vegetation habitats using quad-polarimetric airborne SAR, elevation and optical remote sensing data. *Remote Sens., Environ*. 149, 118–129.

66. **Verma, P., Raghubanshi, A., Srivastava, P.K., Raghubanshi, A.S. (2020).** Appraisal of kappa-based metrics and disagreement indices of accuracy assessment for parametric and nonparametric techniques used in LULC classification and change detection. *Model. Earth Syst. Environ.*, https://doi.org/10.1007/s40808-020-00740-x.

67. **Waser, L.T., Ginzler, C., Kuechler, M., Baltsavias, E., Hurni, L. (2011).** Semi-automatic classification of tree species in different forest ecosystems by spectral and geometric vaiables derived from Airborne Digital Sensor (ADS40) and RC30 data. *Remote Sens. Environ.*, 115,76–85.

68. **Wei, L., Xiangyong, L., Juan D., Yao, L. (2016).** Land cover classification of Radarsat-2 SAR data using convolutional neural network. *Wuhan University Journal of Natural Sciences*, 21(2), 151-158.

69. **Xie, Z., Chen, Y., Lu, D., Li, G., Chen, E. (2019).** Classification of land cover, forest, and tree species classes with ZiYuan-3 multispectral and stereo data. *Remote Sens.*, 11, 164.

70. **Yousefi, S., Mirzaee, S., Tazeh, M., Pourghasemi, H., Karimi, H. (2015).** Comparison of different algorithms for land use mapping in dry climate using satellite images: a case study of the Central regions of Iran. *Desert*, 20(1),1-10.

71. **Yuan, H., Wiele, F.V.D., Khorram, S. (2009).** An Automated artificial neural network system for land use/land cover classification from Landsat TM imagery. *Remote Sens.*, 1, 243-265.

72. **Zakeri, H., Yamazaki, F., Liu W. (2017).** Texture Analysis and land cover classification of Tehran using polarimetric synthetic aperture radar imagery. *Appl. Sci.*, 7, 452.

73. **Zhang, H., Xu, R. (2018).** Exploring the optimal integration levels between SAR and optical data for better urban land cover mapping in the Pearl River Delta. Int. J. Appl. Earth Obs. Geoinf, 64, 87–95.